Title

Observing and modeling the influence of layering on bubble trapping in polar firn

Journal

Journal of Geophysical Research: Atmospheres, 120(6)

ISSN

2169-897X

Authors

Mitchell, Logan E

Buizert, Christo

Brook, Edward J

et al.

Publication Date

2015-03-27

DOI

10.1002/2014jd022766

Peer reviewed

AGU PUBLICATIONS

JGR

Journal of Geophysical Research: Atmospheres

RESEARCH ARTICLE
10.1002/2014JD022766

Key Points:
- Gas occlusion and firn layering are observed in high-resolution measurements
- We present an improved porosity parameterization that accounts for layering
- Understanding layering is important for interpretation of ice core gas records

Supporting Information:
- Texts S1–S4 and Figures S1–S6

Correspondence to:
L. E. Mitchell,
logan.e.mitchell@gmail.com

Citation:
Mitchell, L. E., et al. (2015), Observing and modeling the influence of layering on bubble trapping in polar firn, *J. Geophys. Res. Atmos.*, *120*, 2558–2574, doi:10.1002/2014JD022766.

Received 26 OCT 2014
Accepted 20 FEB 2015
Accepted article online 26 FEB 2015
Published online 28 MAR 2015

Observing and modeling the influence of layering on bubble trapping in polar firn

Logan E. Mitchell[1,2], Christo Buizert[1], Edward J. Brook[1], Daniel J. Breton[3,4], John Fegyveresi[5], Daniel Baggenstos[6], Anais Orsi[6,7], Jeffrey Severinghaus[6], Richard B. Alley[5], Mary Albert[8], Rachael H. Rhodes[1], Joseph R. McConnell[9], Michael Sigl[9], Olivia Maselli[9], Stephanie Gregory[8], and Jinho Ahn[10]

[1]College of Earth Ocean and Atmospheric Sciences, Oregon State University, Corvallis, Oregon, USA, [2]Department of Atmospheric Sciences, University of Utah, Salt Lake City, Utah, USA, [3]Department of Physics and Astronomy, University of Maine, Orono, Maine, USA, [4]Climate Change Institute, University of Maine, Orono, Maine, USA, [5]Department of Geosciences, and Earth and Environmental Systems Institute, Pennsylvania State University, University Park, Pennsylvania, USA, [6]Scripps Institution of Oceanography, University of California, San Diego, La Jolla, California, USA, [7]Laboratoire des Sciences du Climat et de l'Environnement, CEA-CNRS-UVSQ, Gif-sur-Yvette, France, [8]Thayer School of Engineering, Dartmouth College, Hanover, New Hampshire, USA, [9]Desert Research Institute, Nevada System of Higher Education, Reno, Nevada, USA, [10]School of Earth and Environmental Sciences, Seoul National University, Seoul, South Korea

Abstract Interpretation of ice core trace gas records depends on an accurate understanding of the processes that smooth the atmospheric signal in the firn. Much work has been done to understand the processes affecting air transport in the open pores of the firn, but a paucity of data from air trapped in bubbles in the firn-ice transition region has limited the ability to constrain the effect of bubble closure processes. Here we present high-resolution measurements of firn density, methane concentrations, nitrogen isotopes, and total air content that show layering in the firn-ice transition region at the West Antarctic Ice Sheet (WAIS) Divide ice core site. Using the notion that bubble trapping is a stochastic process, we derive a new parameterization for closed porosity that incorporates the effects of layering in a steady state firn modeling approach. We include the process of bubble trapping into an open-porosity firn air transport model and obtain a good fit to the firn core data. We find that layering broadens the depth range over which bubbles are trapped, widens the modeled gas age distribution of air in closed bubbles, reduces the mean gas age of air in closed bubbles, and introduces stratigraphic irregularities in the gas age scale that have a peak-to-peak variability of ~10 years at WAIS Divide. For a more complete understanding of gas occlusion and its impact on ice core records, we suggest that this experiment be repeated at sites climatically different from WAIS Divide, for example, on the East Antarctic plateau.

1. Introduction

Ice cores preserve a unique archive of ancient air that allows us to reconstruct the history of atmospheric trace gases back to 800,000 years ago [e.g., *Loulergue et al.*, 2008; *Luthi et al.*, 2008]. The air trapped in ice sheets is not a direct record of the past atmospheric history, however, because the air must first pass through the porous upper 50–100 m layer of the ice sheet known as the firn where snow progressively transforms into ice. The firn acts as a low-pass filter that attenuates high-frequency atmospheric signals such as the annual cycle of some trace gases [*Buizert*, 2013; *Trudinger et al.*, 1997]. For example, *Spahni et al.* [2003] found that firn smoothing had reduced the magnitude of the methane concentration response to the abrupt 8.2 ka climate event by 34–59% in the EPICA Dome C ice core, a result recently corroborated by *Ahn et al.* [2013]. It is therefore important to understand the processes that affect the atmospheric signal in order to accurately interpret trace gas records measured in ice cores. The two processes that cause smoothing of the atmospheric signal are diffusive transport of air through the open pores and gradual bubble closure that physically traps the air in bubbles at the base of the firn column. Diffusion of air through the open pores has been extensively studied elsewhere [e.g., *Adolph and Albert*, 2013; *Buizert et al.*, 2012; *Schwander et al.*, 1993; *Trudinger et al.*, 1997; *Witrant et al.*, 2012]; this paper will focus on the process of gradual bubble closure.

An interesting paradox is that the bubbles are known to close off over a vertical ice age range that corresponds to roughly 10% of the gas age-ice age difference [e.g., *Schwander et al.*, 1993], which intuitively

should result in a gas age distribution width corresponding to 10% of the gas age-ice age difference. However, the observed smoothing of the trapped gas record often appears to be less than would be expected from this rate of gradual bubble closure. For example, in the low-accumulation Dome C ice core, the abrupt rise in atmospheric methane (CH_4) associated with each Dansgaard-Oeschger event happens within as little as 50 years (the sampling resolution of the record), which is less than 2% of the glacial Dome C gas age-ice age difference [*Loulergue et al*., 2008]. This suggests that other poorly understood processes exist that limit the extent of smoothing. A better insight into these processes is needed, motivating this study.

The firn column is commonly divided into three zones that are defined by the dominant mechanism of air transport. From top to bottom, these zones are the convective zone, the diffusive zone, and the lock-in zone [*Sowers et al*., 1992]. The convective zone contains air that is well mixed with the overlying atmosphere. This zone is typically less than 5 m thick except in very windy locations [*Kawamura et al*., 2006] or in the situation where extremely low accumulation allows deep cracks to form in the firn [*Severinghaus et al*., 2010]. In the diffusive zone, air movement is dominated by molecular diffusion, and the effective diffusivity decreases with depth as the pore volume decreases and the pore space becomes increasingly tortuous. Vertical diffusion of air effectively ceases at the lock-in depth (LID); it has been suggested that the LID corresponds to the depth of the first impermeable, high-density layer [*Battle et al*., 1996]. Below the LID extends the lock-in zone (LIZ), in which advection with the surrounding ice dominates the air transport. There may be a finite amount of remnant diffusivity within the LIZ, the nature of which is poorly constrained by observations [*Buizert et al*., 2012]. At the base of the LIZ, all of the air has been trapped in bubbles within the ice and we refer to this as "mature ice."

Air-entrapment and bubble closure processes are not understood as well as air transport through open pores. Pycnometric measurements of the volume of closed pores have shown that the process of bubble closure occurs gradually and is strongly correlated with density (ρ) [*Schwander et al*., 1993; *Trudinger et al*., 1997]. These measurements have provided the best constraint on the depth where bubble closure occurs at any given firn site; however, recent work suggests that accumulation rate and microstructure may play a role in bubble closure as well [*Gregory et al*., 2014]. While variability in local density with depth (i.e., centimeter-scale layering) is ubiquitous in polar firn, the mechanisms by which it is created and sustained are not fully understood [*Hörhold et al*., 2011]. High-resolution density measurements reveal a characteristic pattern with depth: the magnitude of density variability is largest near the surface, reaches a minimum around densities of 600 to 650 kg m^{-3}, then increases again to reach a second relative maximum [*Gerland et al*., 1999; *Hörhold et al*., 2011]. While layering in the upper firn is due to (near-) surface processes such as deposition variability, wind scouring, and hoar formation, the density variability at depth is the subject of ongoing debate. Explanations include firn softening by layered impurities [*Freitag et al*., 2013; *Hörhold et al*., 2012] and microstructure dependent densification rates [*Freitag et al*., 2004; *Gerland et al*., 1999; *Gregory et al*., 2014; *Hörhold et al*., 2011]. The importance of layering to bubble trapping was realized early on in ice core research [e.g., *Raynaud and Whillans*, 1982]. *Martinerie et al*. [1992] noted that at Summit, Greenland, the high-density (winter) layers sealed before (i.e., at a shallower depth than) the low-density (summer) layers. In addition, *Etheridge et al*. [1992] found that the ice age-gas age difference (Δage) at Law Dome, Antarctica, was on average 2 years smaller in denser winter layers than in the summer layers. Although these observations are decades old, a quantitative framework for relating layering in density and bubble trapping to the smoothing of trace gas records is still lacking. This is primarily due to the paucity of trace gas records from the closed pores of the LIZ, and because the records that do exist suffer from contamination from modern air due to postcoring entrapment of air [*Aydin et al*., 2010].

Here we present high-resolution discrete and continuous measurements of methane (CH_4) concentrations as well as air content (V) from the LIZ closed porosity at the West Antarctic Ice Sheet (WAIS) Divide deep ice coring site. These measurements are corrected for contamination from postcoring entrapment of modern air based on the isotopic ratio of N_2 ($\delta^{15}N$) as well as the cut-bubble effect on V from preparing discrete samples for analysis. We also present high-resolution density measurements of the ice. We use these measurements to show that the typical application of bubble closure parameterizations based on mean ice properties leads to slight inaccuracies in the modeled concentration and age of trace gases in the closed pores. We present a new parameterization for bubble closure that accounts for high-frequency layering imparted by density variations in a stochastic sense, providing an improved fit to the data. Finally, implications of this work and future recommendations are discussed.

2. Methods

2.1. WAIS Divide Site Description

The WAIS Divide ice coring site is located near the West Antarctic Ice Sheet flow divide at 79°28.058′S, 112°05.189′W (surface elevation 1766 m). The modern accumulation rate is $\sim 200 \pm 34\ \mathrm{kg\ m^{-2}\ yr^{-1}}$ [*Banta et al*., 2008], and the mean annual temperature is −30°C [*Orsi et al*., 2012]. The measurements presented here came from a 298 m shallow core extracted in the austral summer of 2005/2006 (WDC05A) 1.3 km northwest of the main borehole (WDC06A). The WDC05A core was dry-drilled with a 10 cm diameter electromechanical drill and had excellent core quality.

2.2. Sample Integrity

Methods for retrieving trace gas and total air content measurements involve placing samples in a high vacuum chamber for approximately 1 h, which removes the ambient air and any remaining air in the open porosity. The samples are then melted and refrozen to release the air trapped in the closed porosity into the headspace, which is then measured by the methods described below. Previous investigators have hypothesized that subjecting firn samples to a high vacuum would cause some of the recently closed air bubbles to break open, since they could have very thin ice walls and the pressure difference between the inside and outside of the bubble would be large [e.g., *Schwander and Stauffer*, 1984; *Stauffer et al*., 1985]. We have no direct way to confirm or reject this hypothesis but instead point to model-data agreement described below between our data and measurements made on other cores without a vacuum system, suggesting that bubble breaking under vacuum was small or negligible.

2.3. CH_4

Air from 182 discrete ice core samples was extracted using a typical wet-extraction technique, and the methane concentrations were then measured by injection into a gas chromatograph (GC) equipped with a flame ionization detector. The methods are described in detail elsewhere [*Mitchell et al*., 2013, 2011]. We measured 26 low-resolution samples (cross-sectional area of 2.5 cm × 2.5 cm, length of ~10 cm) from 11 different depths and 156 high-resolution samples (cross-sectional area of 2.5 cm × 8 cm, length of ~3 cm). The low-resolution sample orientation is typical for mature ice core samples because it allows for 2–4 ice samples with identical depths, whereas the high-resolution sample orientation allows for only one sample from each depth range. Since the mean annual layer thickness in the LIZ is $24 \pm 5\ \mathrm{cm\ yr^{-1}}$, we were able to obtain ~eight samples per annual layer using the high-resolution sample orientation versus only ~2.4 samples per annual layer using the low-resolution sample orientation.

Our previously reported analytical uncertainty for CH_4 samples is ± 2.4 ppb based on the pooled standard deviation of replicate samples on mature ice (i.e., ice below the firn) [*Mitchell et al*., 2013] that have a mean *V* of 111.5 mL of air per kg of ice ($\mathrm{mL\ kg^{-1}}$ in the remainder of the text). However, the high-resolution LIZ samples presented here were not measured in replicate because of limited ice availability, and so we cannot report a pooled standard deviation for this data set. We expect that measurements of samples with lower *V* are slightly less precise, because the concentrations derived from repeated expansions of the sample into the GC have a slightly larger standard error for these LIZ samples (1.6 ppb) than for samples from mature ice (1.2 ppb) with higher *V*. We therefore estimate that our analytical uncertainty is similar to typical ice core samples but slightly higher for samples with lower *V*.

Routine corrections for system blank, solubility (by applying a correction factor of 1.017 to the concentration data), and gravitational fractionation are applied to the discrete CH_4 data following *Mitchell et al*. [2011]. We have also estimated a correction for postcoring bubble closure based on $\delta^{15}N$ of N_2 (supporting information Text S1).

In addition to discrete CH_4 samples, we also measured CH_4 simultaneously with trace element analysis using a continuous technique [*Rhodes et al*., 2013; *Stowasser et al*., 2012]. The samples for this analysis were smaller (3 × 3 × 22 cm) than has been typically used (3.4 × 3.4 × 55 cm), yet this provides a unique opportunity to compare the continuous technique to discrete measurements on samples within the LIZ. The continuous data have been corrected for solubility by applying a correction factor of 1.079 to the concentration data as described by *Rhodes et al*. [2013]. A comparison between the discrete and continuous data is shown in Figure S5 and discussed in the supporting information Text S2.

2.4. Total Air Content

Total air content (V) measurements were obtained simultaneously with the discrete methane measurements. To measure V, we used the sample weight, pressure measurements, the volume of the vacuum flasks and vacuum line, and the temperature of the vacuum line to determine V at standard temperature and pressure in units of mL kg^{-1}. The weight of each sample was determined using an electronic balance with a precision of 0.1 g. The volumes of the flask and extraction line were determined by expanding air from a large flask with a known volume at a constant room temperature. The flask and extraction line were not isothermal, so we calculated the effective temperature (T_e) according to the following equation:

$$T_e = \frac{[(T_{GC} \cdot V_{GC}) \cdot (1 - c)] + [(T_f \cdot (V_f - V_s) + T_l \cdot V_l) \cdot c]}{V_{GC} + V_f - V_s + V_l} \quad (1)$$

where T_{GC}, T_f, T_l are the temperature of the GC oven containing the sample loop (50°C), the flask (i.e., the measured ethanol bath temperature), and the exposed portion of extraction line (room temperature, ~22°C); V_{GC}, V_f, V_s, and V_l are the volumes of the GC, flask, sample, and extraction line; and c is a dimensionless constant. V_s is derived by $V_s = M_{sample}/\rho_{ice}$ where $\rho_{ice} = 917$ kg m^{-3}. The dimensionless constant c represents the relative contribution of T_f and T_l versus T_{GC} to the T_e of the entire extraction line. We adjusted c so that our V results were consistent with those obtained using a different method which utilized a known temperature and pressure [*Lipenkov et al*., 1995; *Martinerie et al*., 1994]. To calibrate c, we first determined the expected V corrected for the cut-bubble effect at WAIS Divide and in a Greenlandic ice core (GISP2), based on the relationship between site temperature and cut-bubble corrected V [*Delmotte et al*., 1999; *Martinerie et al*., 1994]. We then adjusted c until the difference between the expected cut-bubble corrected V (at GISP2 and WAIS Divide) and the cut-bubble corrected V from mature ice (mean of samples from 100 to 300 m at GISP2 and WAIS Divide) was minimized (not shown). The value of c was recalibrated when changes were made to the configuration of the extraction line [*Mitchell et al*., 2013]. The sample V was then calculated by

$$V = \frac{(V_{GC} + V_f - V_s + V_l) \cdot P_1}{T_e} \cdot \frac{273.15}{760} \Big/ M_{ice} \quad (2)$$

where P_1 was the pressure of the sample when it is expanded into the GC sample loop (in units of torr) and M_{ice} was the mass of the ice sample (kg). We corrected for solubility of air in liquid water by increasing P_1 by 1.3%, which was the percentage of the total amount of air that was trapped in the sample ice during the sample refreezing step. We also applied a correction for postcoring bubble closure based on $\delta^{15}N$ (supporting information Text S1) and for the cut-bubble effect (supporting information Text S3).

The pooled standard deviation of replicate V samples of mature ice from WAIS Divide and GISP2 processed on the same analysis line as the samples presented here is 1.1 mL kg^{-1} ($n = 93$) or ~1.1% of the V (Edwards et al., in preparation). As for the CH_4 samples, we have no replicates from the LIZ; however, it is reasonable to assume that our precision is similar to that from mature ice. This analytical precision is comparable to that of previous work [*Martinerie et al*., 1994; *Raynaud et al*., 1997]; however, since our method relies on calibrating T_e using the V versus site temperature relationship [*Delmotte et al*., 1999], it has an estimated absolute accuracy of ± 5% [*Martinerie et al*., 1994].

2.5. $\delta^{15}N$

We measured the isotopic ratios of $^{15}N/^{14}N$ on 33 samples with depths adjacent to high-resolution CH_4 samples, using a Finnigan MAT Delta V mass spectrometer, with methods detailed in *Petrenko et al*. [2006] and based broadly on *Sowers et al*. [1989]. As with the CH_4 and V measurements, there were no replicates from the LIZ, so we assume that the analytical uncertainty is of the same order of magnitude as in previous work which used the same methods but a different although equivalent mass spectrometer (pooled standard deviation of 0.005‰) [*Severinghaus et al*., 2009]. These measurements were used to provide a correction for contamination from postcoring entrapment of modern air (supporting information Text S1).

2.6. Density

High-resolution density was measured over the whole firn column in the WDC06A ice core as well as along segments of the WDC05A ice core LIZ sample depths presented here at a resolution of 3.3 mm using the Maine Automated Density Gauge Experiment (MADGE) instrument, following the methods described in *Breton et al*. [2009]. MADGE uses a ^{241}Am gamma ray source to measure the density of ice nondestructively.

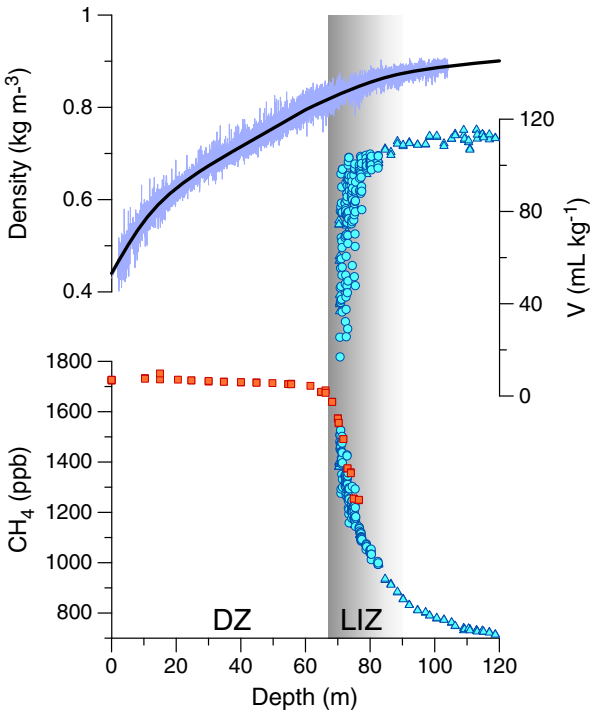

Figure 1. Overview of the firn at WAIS Divide. (top) High-resolution density (ρ, light purple) and mean density ($<\rho>$, black) from WDC06A. (bottom) Air content (V, middle) and CH_4 were measured in the WDC05A core. CH_4 concentrations were measured in air extracted from open pores (orange squares) [*Battle et al.*, 2011] and closed pores (blue circles, this study). Blue circles are high-resolution data (covering 3 cm depth), and blue triangles are low-resolution data (covering 10 cm depth). DZ and LIZ (shaded region) are the diffusive zone and lock-in-zone, respectively.

One meter of the WDC06A data (72.4–73.4) was lost during processing and was reconstructed based on the correlation with optical brightness and the mean density at this depth. The density of the WDC05A LIZ samples was on average lower than the average density observed in WDC06A at equivalent depths. We have therefore increased the WDC05A density by 7.2 kg m^{-3} to correct for this. Analytical uncertainty (1σ) for the density measurements is ± 4.4 kg m^{-3}.

2.7. Chemistry

Trace element analysis was conducted on the LIZ samples using a continuous ice core melter connected to two high-resolution inductively coupled plasma mass spectrometers, which measure trace elements such as Na, Mg, S, Ca, Mn, Rb, Sr, La, Ce, and Pb, as well as spectrophotometers and fluorometers for measuring ammonium, nitrate, and other compounds [*McConnell*, 2002], and a laser-based atmospheric analyzer for measuring black carbon (BC) using methods described elsewhere [*McConnell et al.*, 2007].

2.8. Model Description

To interpret the measurements we used the Center for Ice and Climate, University of Copenhagen, firn air transport model [*Buizert et al.*, 2012]. The model solves the second order diffusion-advection equation in a Eulerian (i.e., static) reference frame using implicit Crank-Nicolson time stepping. The physical processes included in the model are convection and wind pumping in the upper firn [*Kawamura et al.*, 2006], molecular diffusion, downward advection with the ice matrix, dispersive mixing in the deep firn, bubble trapping, and compaction of closed bubbles. We assumed a steady state, isothermal firn at −31°C. Mean annual atmospheric pressure at WAIS is $P = 780$ hPa [*Lazzara et al.*, 2012]. The effective diffusivity with depth was calibrated using seven transport tracers with known atmospheric history (CH_4, CO_2, SF_6, $\delta^{15}N$, CFC-11, CFC-12, and HFC-134a) [*Battle et al.*, 2011; *Buizert et al.*, 2012]. The fit to the WAIS firn air data with this model is shown in Figures 5 and S1, as well as elsewhere [*Buizert et al.*, 2013].

3. Results

3.1. Observations

Methane concentrations in the firn air samples have an overall pattern that is similar to that observed elsewhere (Figure 1) [*Battle et al.*, 1996; *Schwander et al.*, 1993; *Witrant et al.*, 2012]. Within the diffusive zone, concentrations are nearly constant due to rapid transport of air and the relatively stable atmospheric concentrations over the decade prior to drilling. The lock-in depth (LID) is found at $z_{LID} = 67$ m [*Battle et al.*, 2011], below which the CH_4 concentrations decrease quickly with depth, reflecting both the rapidly increasing atmospheric CH_4 burden prior to 1998, as well as the slow LIZ transport that is dominated by advection (Figure 1).

The isotopic ratio of N_2 ($\delta^{15}N$) is a sensitive tracer for postcoring entrapment of modern air (supporting information Text S1). We measured $\delta^{15}N$ in 33 of our shallower samples (70.75–73.15 m) which have the

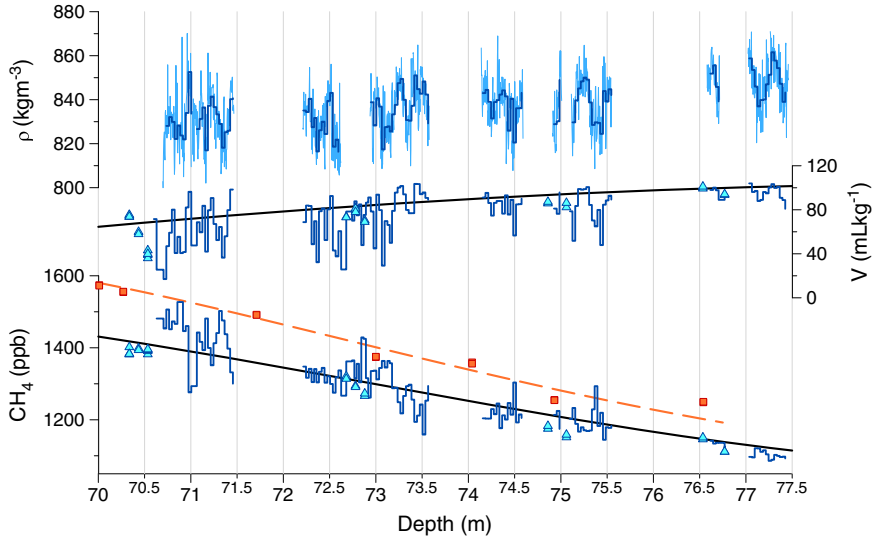

Figure 2. (top) Density, (middle) air content (*V*), (bottom) and methane (CH_4) from WDC05A. The raw density measurements are shown with the light blue line, and the average density over the depth of the high-resolution CH_4 samples is shown by the dark blue line. High-resolution (covering 3 cm depth) CH_4 and *V* measurements are shown by the dark blue lines. Low-resolution (covering 10 cm depth) CH_4 and *V* measurements are triangle symbols. The CH_4 measurements are corrected for blanks, solubility, gravitational fractionation, and postcoring bubble closure. The smooth black lines show the spline fit to the WDC06A density (top), and modeled results for *V* (middle) and CH_4 (lower). CH_4 measurements (orange symbols) [*Battle et al.*, 2011] and model (orange dashed line) for the open porosity are also shown.

greatest amount of open porosity and therefore the greatest likelihood of postcoring entrapment of modern air. The results show convincing evidence for postcoring entrapment of modern air. Based on a mass balance calculation, $10.6 \pm 6.1\%$ of the air in these samples came from modern air (supporting information Text S1). Furthermore, there is a strong correlation between the *V* in the sample and the percent of modern air contamination, with samples that contain less air having more contamination and vice versa. We hypothesize that this is because samples with less trapped air have a greater proportion of open porosity and, therefore, a greater opportunity for postcoring trapping of modern air. We used the linear regression of this relationship to derive a correction for postcoring contamination for our CH_4 and *V* samples (supporting information Text S1 and Figure S3).

Our *V* and CH_4 measurements exhibit variability that is indicative of nonuniform trapping with depth (Figure 2). They are anticorrelated ($r = -0.44$, $p < 0.01$), consistent with the interpretation that layers containing more air closed off at an earlier time, thereby sampling older air with lower CH_4 concentrations (Figure 2 and supporting information Text S1). The magnitudes of the variability about the mean are notably large. The *V* variations of 60–80 mL kg^{-1} can be compared with the mean and standard deviation in mature ice of 112 ± 2 mL kg^{-1} (from 100 to 200 m). The methane variations of 100–200 ppb are observed in both discrete and continuous measurements (Figures 2 and S5) and can be compared to the annual rate of methane increase during the past half century of ~10–17 ppb yr^{-1} [*Etheridge et al.*, 1998]. These large variations imply that adjacent samples (~3 cm apart) have mean gas ages ~10 years different from each other, despite having ice ages of only a few months apart. Note that the annual cycle of ~30 ppb should not be visible within the LIZ due to smoothing in the diffusive column [*Trudinger et al.*, 1997], and that this cannot be the origin of the observed variability. Similar variations are observed in the LIZ from a new methane record from the North Greenland Eemian ice core (NEEM-2011-S1) using the same continuous melting system as used here [*Rhodes et al.*, 2013]. Those NEEM variations have a quasi-annual frequency and are anticorrelated with concentrations of Ca, typically used as a dust proxy. Some of the continuously sampled CH_4 measurements have a higher concentration than those found in the open pores of NEEM firn extracted in 2008 and so must be influenced by an unknown fraction of modern air that was assimilated either during the melting process or from postcoring entrapment of modern air. Based on the comparison between continuous and discrete samples, it is likely that most of the observed variability in the NEEM-2011-S1 data is a result of the bubble trapping processes.

We also measured the density of ice adjacent to our high-resolution CH_4 and V samples. The density measurements have a resolution of 3.3 mm, and in Figure 2 we show these as well as the mean density over the discrete sample depth intervals. There is a high correlation between the mean sample density and V ($r = 0.87$, $p < 0.01$, Figure 2), discussed in greater detail below.

Observations of a positive correlation between Ca and density at depth within the firn have led to the hypothesis that trace impurities induce softening of the firn and cause faster densification rates [*Freitag et al*., 2013; *Hörhold et al*., 2012]. We therefore examined the correlations between trace elements and local density in our LIZ samples, and found some statistically significant results ($p < 0.01$): Mg ($r = 0.40$), Sr ($r = 0.37$), Ca ($r = 0.19$), BC ($r = 0.17$), Na ($r = 0.14$), S ($r = -0.16$), and HNO_3 ($r = -0.23$). These results appear consistent with those from *Hörhold et al*. [2012]; however, we caution that since our samples covered only a limited portion of the LIZ, were discontinuous, were not the ideal size for processing on the melter system, and had relatively low (albeit significant) correlations, the conclusions that we can draw from these data are limited.

3.2. A Stochastic Description of Bubble Trapping in Layered Firn

Traditionally, firn air models use the mean properties of the firn and ignore firn layering. Here we use the high-resolution density profile from WDC06A [*Kreutz et al*., 2011] that resolves firn layering on subannual resolution. We used the density profile from WDC06A because the high-resolution density was measured over the whole firn column, whereas in WDC05A it was only measured on the LIZ samples presented here. In the following discussion, we distinguish between the layered density profile $\rho(z)$ as it exists at a given moment in time and the averaged density profile $<\rho(z)>$, which is assumed stationary on time scales considered here. We shall refer to ρ and $<\rho>$ as the local and bulk densities, respectively. The bulk densities $<\rho(z)>$ used here are obtained from a smoothed spline fit to the high-resolution local density measurements from WDC06A as a function of depth (Figure 1). The same distinction is made for the porosity, where we have the local porosity $s = 1 - \rho/\rho_{ice}$ and the bulk porosity $<s> = 1 - <\rho>/\rho_{ice}$. The porosity is a combination of open and closed pores ($s = s_{op} + s_{cl}$), with the former still interconnected with each other and the overlying atmosphere and the latter consisting of isolated bubbles. Two parameterizations of closed porosity can be found in the literature, the first by [*Schwander*, 1989]

$$s_{cl} = \begin{cases} s \cdot \exp[\lambda(\rho - \rho_{co})] & \text{for } \rho < \rho_{co} \\ s & \text{for } \rho \geq \rho_{co} \end{cases} \tag{3}$$

with $\lambda = 75/\rho_{co}$ and the close off density $\rho_{co} = 830\ \mathrm{kg\ m^{-3}}$ at Summit station, Greenland. A slightly modified version of the Schwander parameterization is given in *Severinghaus and Battle* [2006]. The second is the Barnola parameterization [*Goujon et al*., 2003]

$$s_{cl} = 0.37 \cdot s \cdot \left(\frac{s}{\overline{s_{co}}}\right)^{-7.6}$$

with

$$\overline{s_{co}} = 1 - \overline{\rho_{co}}/\rho_{ice} \tag{4}$$

$$\overline{\rho_{co}} = \left(\frac{1}{\rho_{ice}} + 6.95 \cdot 10^{-7} T - 4.3 \cdot 10^{-5}\right)^{-1},$$

where $\overline{s_{co}}$ is the mean close off porosity, and $\overline{\rho_{co}}$ is the mean close off density [*Martinerie et al*., 1992, 1994]. Note that the close off density (ρ_{co}) in equation (3) has a slightly different meaning and value from the mean close off density ($\overline{\rho_{co}}$) in equation (4).

It is important to remember that both parameterizations were derived from porosity measurements on centimeter-scale samples and, therefore, give a relationship between local s_{cl} and local ρ. Like the local firn density, the local closed porosity and V exhibit strong variability with depth due to layering. This is illustrated in Figure 3 for the Greenland Summit, Antarctic DE08 (Law Dome), and WDC05A ice cores. Figure 3 (left column) shows the fraction of closed pores and V in a sample (s_{cl}/s, V/V_{mature}) as a function of the (local) sample density. There is little scatter in the data, indicating that local density is an excellent predictor of bubble closure and V (since V is directly related to the closed pore volume after correction for increased pressure due to bubble compaction). When the same data are plotted versus the bulk density at sampling depth (Figure 3, right column), we observe strong scatter due to layering (the bulk density is proportional to

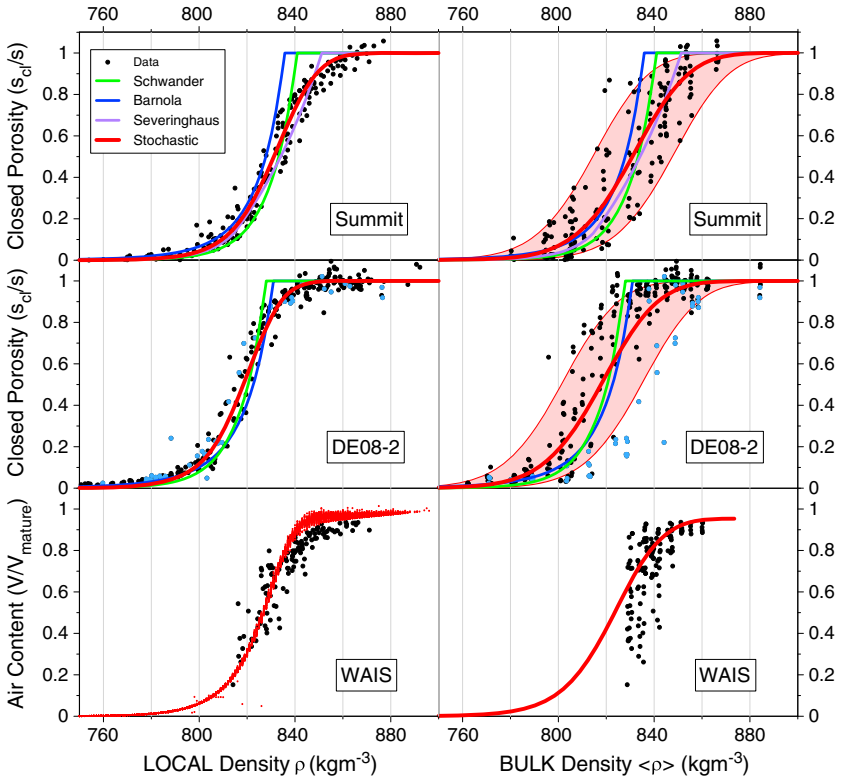

Figure 3. Parameterizations for closed porosity and air content (V) compared with closed porosity measurements at Summit, Greenland [*Schwander et al.*, 1993] and DE08-2, Law Dome, Antarctica [*Trudinger et al.*, 1997] and V at WAIS Divide (this work). The closed porosity data are all increased by 7% to account for the cut-bubble effect (causing some of the data to be greater than 1), and the V data are corrected with a spline fit to cut-bubble observations from digitized thin sections (supporting information Text S3). At DE08-2, the black dots are from winter layers and the light blue dots are from summer layers. (left column) Fraction of closed pores versus sample (i.e., local) density; red curves follow equation (5) where we include a measurement error σ_{meas} (supporting information Text S4), and red dots show calculated V as indicated in Figure 4c and described in the text. (right column) Fraction of closed pores versus bulk density at sampling depth; red curves show equation (6) where we calculate σ_{layer} using ρ between 60 and 80 m ($\sigma_{layer} = 12$ kg m^{-3} at Summit and $\sigma_{layer} = 13$ kg m^{-3} at DE08-2, as obtained from equation (9)) and include a measurement error σ_{meas} (supporting information Text S4). Bulk density ($<\rho>$) is obtained with a spline fit to local density (ρ) data. Green lines show equation (9) applied to ρ (left column) and to $<\rho>$ (right column). In all parameterizations, we use $\rho_{co} = 841$ kg m^{-3} at Summit, $\rho_{co} = 828$ kg m^{-3} at DE08-2, and $\rho_{co} = 837$ kg m^{-3} at WAIS Divide. The modified Schwander parameterization [*Severinghaus and Battle*, 2006] (purple line) and Barnola parameterization [*Goujon et al.*, 2003] (blue line) are also shown.

depth given the monotonic depth-$<\rho(z)>$ relationship). At the high-accumulation DE08 site, it is possible to clearly distinguish between summer (light blue dots) and winter (black dots) layers [*Martinerie et al.*, 1992]. On average, (lower density) summer layers close off deeper than the (higher density) winter layers do at DE08.

For modeling purposes the effect of layering is commonly neglected, and the bulk firn properties are used instead of the local ones. For example, in firn air modeling the firn properties are assumed stationary [e.g., *Trudinger et al.*, 1997]; this is a necessary assumption given the strong spatial and temporal variability of real firn. It is common practice to start from $<\rho>$ to obtain $<s>$ and then use these bulk properties in equations (3) and (4) to obtain bulk $<s_{cl}>$. We want to point out that this approach is strictly speaking invalid, given that the parameterizations were derived on local properties and cannot be expected to apply to bulk properties as well. The correct approach would be to start from high-resolution ρ measurements to obtain local s_{cl} values, which can subsequently be averaged to find $<s_{cl}>$. This difference is subtle but important. The strong layering of firn causes the first bubbles to close off before this is expected based on $<\rho>$ alone and allows for open pores to be present when $<\rho> \geq \rho_{co}$. The (incorrect) application of equations (3) and (4) to bulk properties has only a minor impact on the modeling of trace gas concentrations in the open porosity because (i) the bubble trapping process itself does not alter trace gas mixing ratios in the open pores, and (ii) firn air models are

calibrated to trace gases of well-known atmospheric history. We therefore do not mean to suggest that previous firn air modeling studies are invalid. However, when modeling trace gas concentrations in the closed pores, the depth of bubble trapping is of the greatest importance and incorrect use of equations (3) and (4) will lead to errors as we demonstrate.

We now present a new closed porosity parameterization that (i) provides an improved fit to existing measurements of (local) closed porosity and (ii) includes the effect of firn layering on bubble trapping in a stochastic sense. The Schwander parameterization of equation (3) is given by the green line in Figure 3, and it appears that the parameterization closes bubbles too abruptly; this was also noted by *Severinghaus and Battle* [2006], who modified the Schwander parameterization to make the close off process more gradual (Figure 3, purple line). The Schwander equation can be interpreted as the probability density function of an exponential distribution of the random variable $u = \lambda(\rho_{co} - \rho)$. The abrupt ending of the Schwander parametrization is due to the fact that ρ_{co} is considered constant. Instead, we consider u to have a Gaussian distribution of standard deviation $v = \lambda \cdot \sigma_{co}$, taking into account the variability in the close off density (σ_{co}). This leads us to replace equation (3) with a cumulative distribution function of an exponentially modified Gaussian distribution. This equation is commonly used to characterize peaks in gas chromatography [e.g., *Kalambet et al.*, 2011] and can also be described as having a functional form of the exponential Schwander parameterization convolved with a Gaussian function. It is expressed here as follows:

$$s_{cl} = s \cdot \left(1 - \Phi(u, 0, v) + \exp\left[-u + \frac{v^2}{2} + \ln\left\{\Phi\left(u, v^2, v\right)\right\}\right]\right) \tag{5}$$

with

$$\Phi(x, \mu, \Sigma) = \frac{1}{2} + \frac{1}{2}\,\mathrm{erf}\left(\frac{x - \mu}{\sqrt{2\Sigma^2}}\right)$$
$$u = \lambda(\rho_{co} - \rho)$$
$$v = \lambda \cdot \sigma_{co},$$

where erf(.) denotes the error function and $\lambda = 75/\rho_{co}$ as before. Contrary to equation (3), this parameterization is valid for all ρ and is differentiable at ρ_{co}. The best fit to DE08 and Summit data (red curve in Figure 3, left column) is observed for $\sigma_{co} = 7\ \mathrm{kg\,m^{-3}}$ (supporting information Text S4); close off densities are given in the figure caption and were chosen to optimize the fit. When fitting the data, it is important to consider the measurement uncertainties; details of the fitting procedure are outlined in supporting information Text S4. In the limit $\sigma_{co} \to 0$, equation (5) is equal to the Schwander parameterization (equation (3)). The parameter σ_{co} describes the intrinsic smoothness of the bubble close off process in a local sense and is not directly linked to density layering.

Although lacking the mathematical simplicity of other porosity parameterizations, the form of equation (5) allows us to easily include the effects of layering on bulk firn parameters in a stochastic sense. We assume that $\rho(z)$ is a stochastic variable with mean value $<\rho(z)>$ and standard deviation σ_{layer} due to layering. Local density variability is normally distributed about the mean bulk density, so a Gaussian functional form adequately describes its stochastic nature. The bulk closed porosity can now be obtained by convolving equation (5) with a Gaussian of width σ_{layer}, giving

$$< s_{cl} > = < s > \cdot \left(1 - \Phi(u, 0, v) + \exp\left[-u + \frac{v^2}{2} + \ln\left\{\Phi\left(u, v^2, v\right)\right\}\right]\right) \tag{6}$$

with $v = \lambda \cdot \sqrt{\sigma_{co}^2 + \sigma_{layer}^2}$ and Φ, u as in equation (5). Note that equation (6) is nearly identical to equation (5), the difference being that local properties s and s_{cl} are replaced by bulk properties $<s>$ and $<s_{cl}>$, and that the width of the distribution has increased from σ_{co} to $\left(\sigma_{co}^2 + \sigma_{layer}^2\right)^{1/2}$ to account for layering. By setting $\sigma_{co} = 0$ in equation (6), one obtains the Schwander parameterization corrected for density layering. The fit of equation (6) to DE08 and Summit data is shown in Figure 3 (right column), where σ_{layer} was derived from density measurements at the sites between 60 and 80 m, and we also include an estimate of sampling and measurements uncertainty (σ_{meas}, see supporting information Text S4 for details). The shaded area indicates the magnitude of the layering at both sites, given by $\left(\sigma_{co}^2 + \sigma_{layer}^2 + \sigma_{meas}^2\right)^{1/2}$. *Severinghaus and Battle* [2006] modified the Schwander equation to better describe the enrichment of fugitive gases ($\delta O_2/N_2$, $\delta Ar/N_2$, and $\delta Ne/N_2$) in the open porosity of the LIZ (Figure 3). Their result agrees fairly well with our

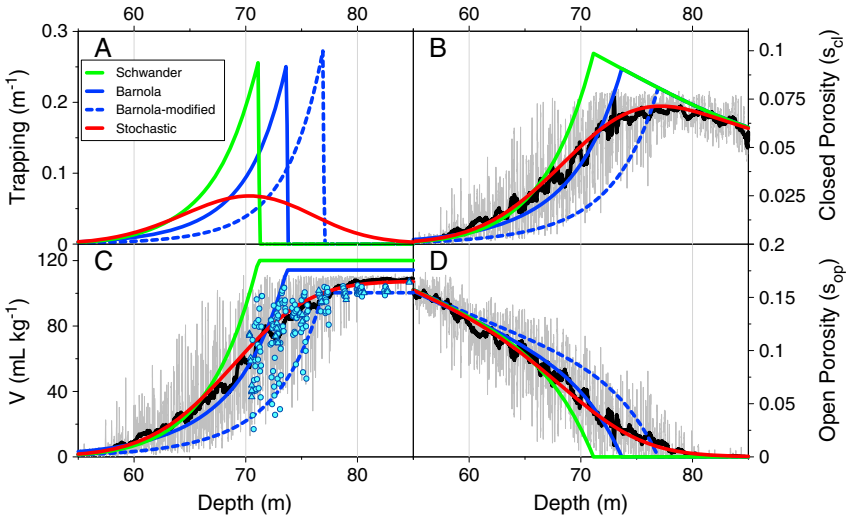

Figure 4. Porosity parameterizations applied to the WAIS site. The Schwander, Barnola, modified Barnola, and equation (6) parameterizations use $\rho_{co} = 830$ [*Schwander*, 1989], $\overline{\rho_{co}} = 0.6$ [*Martinerie et al.*, 1994], $\overline{\rho_{co}} = 836$, and $\rho_{co} = 837$ kg m^{-3}, respectively. (a) Trapping rate d($<s_{cl}>/<s>$)/dz. (b) Closed and (d) open porosities, with local s_{cl} and s_{op} reconstructed from $\rho(z)$ using equation (5) in light grey and a 200 point running average (dark grey). (c) Air content (V), with local V (light grey), running mean V (dark grey), and high-resolution V data (blue circles). V in the model is calculated as $s_{cl} \cdot P_{cl}/1013.25 \cdot 273.15/T \cdot \rho^{-1}$, where P_{cl} is the mean pressure in closed bubbles, which exceeds the open pore pressure due to continued pore compaction after close off; see *Buizert* [2011] for details.

equation (6), leading us to speculate that our parameterization would work well with the permeation model implemented in *Severinghaus and Battle* [2006]. When detailed closed porosity or air content data are unavailable at a given site, we recommend the following parameters be used in equations (5) and (6):

$$\rho_{co} = \frac{1}{1 - 1/75} \cdot \left(\frac{1}{\rho_{ice}} + 7.02 \cdot 10^{-7} T - 4.5 \cdot 10^{-5} \right)^{-1} \quad (7)$$

$$\sigma_{co} = 7 \text{ kg m}^{-3} \quad (8)$$

$$\sigma_{layer} = \sqrt{\frac{1}{N} \sum_{LIZ} (\rho_i - <\rho>_i)^2}, \quad (9)$$

where T is the temperature (Kelvin), N is the number of data points used in the summation, and i indices are the individual data points. Equation (7) is based on the mean close off density from [*Delmotte et al.*, 1999], corrected for the skewness of the trapping distribution (the mean of the trapping distribution occurs in our parameterization at $\rho_{co} - 1/\lambda$). In Figure 3 we used ρ_{co} values that are different from those calculated with equation (7) to optimize the fit to the porosity data; Equation (7) is therefore recommended when no porosity data are available. Equation (9) gives the standard deviation of (centimeter scale) local density data in the LIZ after subtracting bulk densities. We find that the value of σ_{layer} is mostly insensitive to the exact choice of the depth interval used in equation (9); when using sparse data sets, the depth interval can be increased to obtain a statistically robust value.

We now apply the new parameterization to the WAIS Divide site. Because we have no porosity data at WAIS Divide, we use equations (7)–(9) to find $\rho_{co} = 837$ kg m^{-3} and $\sigma_{layer} = 12.5$ kg m^{-3} obtained from the $\rho(z)$ data in Figure 1 over the 60–80 m depth interval. In Figure 4, we compare equation (6) to the Schwander and Barnola parameterizations. As we mentioned earlier, it is incorrect to use the $<\rho>$ in the latter two parameterizations, and here we do it only because it is the common practice in the literature. Using the Schwander and Barnola parameterizations, we get full bubble closure ($s_{op} = 0$) around 71.5 and 74 m depth, respectively (Figure 4d). This is incompatible with the field observation that it was possible to pump air from the open porosity of the firn to a depth of 76.5 m, indicating that substantial interconnected pore space must still exist below 74 m [*Battle et al.*, 2011] (Figure 2). Therefore, we added a modified Barnola parameterization (blue dashed line) for which the mean close off porosity $\overline{s_{co}}$ in equation (4) was adjusted

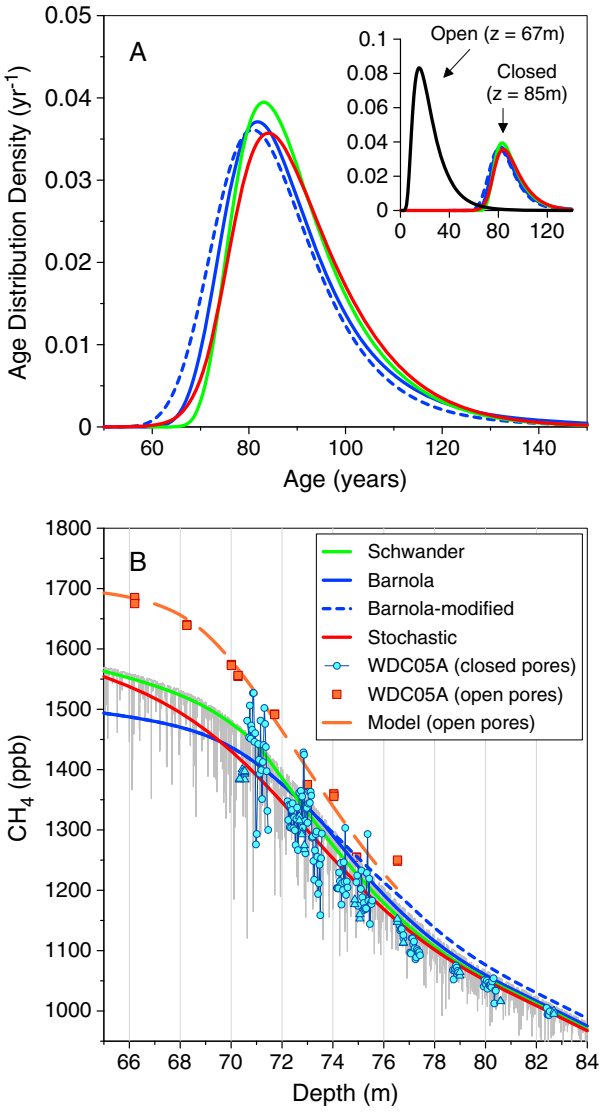

Figure 5. (a) Age distribution of CH_4 in closed pores at the base of the LIZ as well as (b) CH_4 concentration observation and model results using the different parameterizations. Inset shows the age distribution in the open porosity at the LID ($z = 67$ m) as well as the closed porosity at the base of LIZ ($z = 85$ m). The green, blue, blue dashed, and red lines show the modeled age distribution and CH_4 in the closed porosity using the Schwander, Barnola, Barnola-modified, and Stochastic parameterizations, respectively. Blue circles are the high-resolution measurements, and blue triangles show the low-resolution measurements (as in Figure 2). Light grey line shows the modeled CH_4 using the high-resolution WDC06A density data. CH_4 measurements (orange symbols) [*Battle et al.*, 2011] and model (orange dashed line) for the open porosity are also shown.

to yield full bubble closure at 77 m depth; this adjustment is commonly made in firn air modeling studies [e.g., *Buizert et al.*, 2012; *Witrant et al.*, 2012] that focus on the modeling of trace gases in the open porosity alone.

Figure 4a shows the bubble trapping rate $d(<s_{cl}>/<s>)/dz$. It is clear that our method gives gas occlusion over a much wider depth range than the other parameterizations. Because $\sigma_{layer} > \sigma_{co,}$ the broadening is mostly caused by including the layering (in a stochastic sense). Also, our trapping distribution is smooth and does not show a discontinuity at the close off depth. While the modification to the Barnola parameterization is commonly made for modeling trace gases in the open porosity, this modification causes the mean depth of the bubble trapping to occur much deeper than with the other parameterizations.

Figures 4b and 4d show the closed and open porosities, respectively. The light grey line gives local $s_{cl}(z)$ and $s_{op}(z)$ calculated from the high-resolution $\rho(z)$ data from WDC06A using equation (5), with a 200 point moving average shown in dark grey. Contrary to the common practice of applying the classical parameterizations on bulk density, the $s_{cl}(z)$ and $s_{op}(z)$ curves shown in light and dark grey do not show a sudden close off horizon below which no open pores exist; note that this is a consequence of the layering, and that the same result would have been found irrespective of which closed porosity parameterization is used since we are examining density and porosity at the local scale (see the difference between the parameterizations in Figure 3, left column). Both the reconstructed $s_{op}(z)$ and our $<s_{op}>$ curve have finite open porosity at 76.5 m depth, in agreement with the deepest firn air sample extraction. This means our parameterization can be used in firn air modeling studies without ad hoc modifications to the closed porosity (such as the modified Barnola parameterization shown here).

In Figure 4c, we plot V with depth. To convert local closed porosity (units of $cm^3\,cm^{-3}$) to local V (units of $mL\,kg^{-1}$), we need to (1) convert the site temperature and pressure to standard temperature and pressure using the ideal gas law, and (2) multiply by the mean closed bubble pressure, which is above ambient as densification compacts bubbles after they have closed. We calculate bubble pressure after *Buizert* [2011], which assumes that the firn column is in steady state, and that closed pores are compacted at the same

Table 1. Age Distribution Characteristics of CH_4 in the Closed Porosity at the Bottom of the LIZ ($z = 85$ m) Including the Mean Age and Spectral Width (Δ A Measure of the Width of the Age Distribution)[a]

Parameterization	Mean	Δ
Barnola	89.9	11.4
Barnola modified	86.9	10.2
Schwander ($\rho_{co} = 830$)	90.5	9.2
Schwander ($\rho_{co} = 837$)	87.8	8.7
Stochastic (this study)	91.0	9.7

[a]All values are given in years.

fractional rate as the total porosity. As in Figures 4b and 4d, the dark grey line in Figure 4c is a 200 point moving average of the calculated local *V*. Using equation (6), we model a final *V* of 108.8 mL kg^{-1}, in good agreement with the 109.4 mL kg^{-1} expected from the linear regression of measured *V* versus site temperature at a range of ice core sites [*Delmotte et al.*, 1999]. Moreover, the amplitude of *V* variability in the data agrees with our reconstructed local *V* (in light grey in Figure 4c). In Figure 3 (bottom row), we plot the modeled local (left) and bulk (right) *V* versus density in red, which show good agreement with the data in black.

To summarize, our new s_{cl} and $<s_{cl}>$ parameterizations give a good fit to DE08 and Summit closed porosity measurements (Figure 3), reconstructed high-resolution $s_{cl}(z)$ and $s_{op}(z)$ profiles, and LIZ *V* measurements (Figure 4). The site-dependent magnitude of density variability from layering is introduced through a single parameter. Our parameterization is also consistent with the deepest firn air open-porosity sampling depth without the need for ad hoc adjustments.

4. Discussion

4.1. Age Distribution

One important application of our CH_4 and *V* measurements is the experimental verification of the age distribution of air in the closed porosity as originally suggested by [*Schwander*, 1989]. The modeled gas age distribution reflects the integrated impacts of the firn's smoothing properties on a trace gas, and quantification of this is important because it determines the maximum frequency at which the atmospheric signal is recorded in ice cores. Figure 5a shows the CH_4 age distribution in the closed porosity at 85 m, and Figure 5b shows the modeled CH_4 using the four parameterizations. In addition, Table 1 reports the mean age and spectral width (Δ, a measure of the width of the age distribution) [*Trudinger et al.*, 2002] of the age distributions at 85 m.

The differences in concentration calculated with the different parameterizations are large at the top of the LIZ (~67 m) because the Barnola parameterization uses a polynomial form compared to the exponential form by Schwander, causing shallower bubble trapping in the former. However, these differences are not meaningful because the amount of air trapped at this depth is very small, and we do not have any data at this depth to compare with the model results. In the deeper portion of the LIZ, the concentrations from the modified Barnola parameterization are higher than the other parameterization as well as the measurements. This is because the bubble trapping in the modified Barnola parameterization occurs too deeply throughout the LIZ (Figure 4c). Deeper trapping causes the mean age of CH_4 calculated with the modified Barnola parameterization to be ~4 years younger than calculated with our stochastic parameterization (Table 1). With atmospheric growth rates of ~10 ppb yr^{-1} during the past half century, this translates to a modeled CH_4 difference of ~40 ppb, which is observed between the stochastic and Barnola-modified parameterizations through the deeper portion of the LIZ (Figure 5b; root-mean-square errors (RMSE) between the CH_4 observations at ~82 m and the modeled CH_4 concentrations are as follows: Schwander = 6.6; Barnola = 10.6; Barnola modified = 23.3; and Stochastic = 4.7). Our stochastic parameterization appears to have a similar mean age as the Schwander parameterization (Table 1). However, the Schwander parameterization uses $\rho_{co} = 830$ kg m^{-3}, whereas the stochastic parameterization uses $\rho_{co} = 837$ kg m^{-3}. For comparison, Table 1 also gives the mean age and spectral width of the Schwander parameterization using $\rho_{co} = 837$ kg m^{-3}, which provides a more direct comparison with our stochastic parameterization. While the 2–4 year mean age difference between the parameterizations is important for improving the chronologies of high-resolution ice core records, it is smaller than the estimate of the uncertainty of the method (±20 years).

In addition to our stochastic (steady state) firn air transport modeling, we perform a modeling run including the layering in a deterministic sense, basing the bubble trapping on measurements of local ρ rather than the assumption of a Gaussian distribution. To this end, we bin the ρ data into 5 mm layers and assume that for

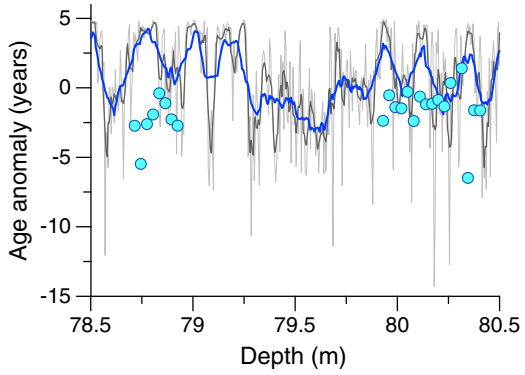

Figure 6. Age anomalies of air at the base of the LIZ. The light grey line is calculated from the 5 mm high-resolution density data, and in addition, we show a 6 point (black) and a 20 point (blue) smoothing curve representing a 3 cm and 10 cm sample, respectively. The calculation of the age of the samples (blue circles) is described in the text. In modeling the local CH_4 age, we used the high-resolution WDC06A density data. We trace the position of each 5 mm layer back in time to estimate an individual trapping history, by assuming the density deviation from the bulk ($\rho - <\rho>$) is preserved throughout the firn-ice transition.

each layer the density anomaly $\rho - <\rho>$ is preserved as the sample traverses the firn. Using equation (5), we covert the density history of each layer into a closed porosity history, which in turn gives the air-trapping history unique to each specific layer, and thereby its gas age distribution and CH_4 concentration. The simulated (local) CH_4 concentrations in the layers (Figure 5b, light grey line) show CH_4 variability comparable to that seen in the data. The variability in the local mean age of the trapped air is shown in Figure 6, where we subtracted the bulk mean age of the air (Figure 5a) to obtain deviations from bulk firn properties. This high-resolution mean age anomaly reconstruction has a resolution of 0.5 cm (light grey line); in addition, we show 6 point (black line) and 20 point (blue line) smoothing curves to represent the magnitude of variability expected in samples spanning a depth of ~3 cm and ~10 cm, respectively. We also calculated the mean age anomaly in our high-resolution CH_4 samples using the Law Dome CH_4 time series to determine the age of the air in our samples then subtracted this age from the mean age of the air modeled with the bulk density curve from WDC06A.

Figure 6 shows that the mean age of air within the LIZ has peak-to-peak variations of ~10 years at the 3 cm scale, consistent with our high-resolution data. Note that the modeling is based on WDC06A density data, whereas the samples are from WDC05A; and therefore, an exact model-data match is not expected. The figure merely indicates that modeling and data give a similar magnitude of mean age variability in adjacent layers. These results are consistent with the observation at DE08 (Law Dome) that summer layers contain air that is ~1.8 years younger than the surrounding winter layers [*Etheridge et al*., 1992], with the smaller variability being a result of the very high accumulation rate (modern accumulation rate at DE08 is ~1100 kg m^{-2} yr^{-1}) that moves ice faster through the LIZ. In addition, *Rhodes et al*. [2013] observed small, quasi-annual variations in mature ice from the NEEM-2011-S1 (Greenland) ice core, which has a similar accumulation rate to WAIS Divide. The variations from ~1550 C.E. occur during a decrease in overall methane concentrations of ~2 ppb yr^{-1}. The peak-to-peak magnitude of these methane fluctuations is ~24 ppb, which indicates that adjacent layers have mean age peak-to-peak variations of ~12 years. The results from these three sites are all consistent with the interpretation that density variability is affecting the mean age of samples, and it confirms that the quasi-annual scale variations observed in continuous methane records are not atmospheric in origin but are instead relics of the stochastic nature of bubble trapping in the layered firn medium [*Rhodes et al*., 2013].

As discussed above, the exact location of the LID is an important feature for understanding the age distribution and spectral width of trace gases. The LID is commonly defined as the depth at which gravitational enrichment of $\delta^{15}N$ ceases, indicating that the density in the firn has increased to a point where vertical diffusion is effectively inhibited, isolating air from the overlying atmosphere. It has not been possible, however, to quantitatively relate the LID to a particular density. We find that the LID at WAIS Divide occurs at $<\rho> = \rho_{co} - 0.77 \times \sigma_{layer}$, and the depth of the deepest open porosity firn air sample is at $<\rho> = \rho_{co} + 0.71 \times \sigma_{layer}$. At WAIS, the LIZ is therefore spanned by a bulk density range of ~$1.5 \times \sigma_{layer}$. We hypothesize that this relationship could hold for other sites as well. This suggests that, mechanistically, the thickness of the LIZ is controlled by the magnitude of density variability (σ_{layer}). This hypothesis is qualitatively supported by other recent observations. *Hörhold et al*. [2011] noted a positive correlation between the magnitude of density variability in the LIZ and site temperature and accumulation rate. Therefore, thicker LIZs should be observed at warmer, high-accumulation sites and thinner LIZs observed at cold, low-accumulation sites, which is consistent with observations from firn air sampling [*Witrant et al*., 2012]. Recently, *Gregory et al*. [2014]

hypothesized that accumulation rate and microstructure may be important for controlling the thickness of the LIZ; however, since the microstructure was not measured on these samples we cannot confirm this hypothesis here.

Similar to the mean ages discussed above, the differences between the spectral widths of the different parameterizations are small (Table 1). The traditional explanation for this is that the slight differences are caused primarily by differing amounts of air being trapped above the LIZ, since once in the LIZ the air is advected with the ice and bubble trapping no longer broadens the gas age distribution. This effect causes the Barnola parameterization to give a wider age distribution in the bubbles than both the Schwander parameterization and our stochastic parameterization because it has shallower trapping, as discussed above. However, a thick LIZ could lead to additional diffusive smoothing of the atmospheric record due to continued gas mixing during the long residence time of gases within the LIZ [*Buizert et al*., 2012]. Future work should examine the impacts of these two processes at sites with a variety of LIZ thicknesses.

4.2. Total Air Content

The final *V* is controlled primarily by the depth at which bubbles seal. Shallow trapping (i.e., with lower ρ and higher total porosity) leads to a higher *V*, and vice versa. The parameterizations each trap bubbles at different depths (Figure 4a), which leads to variable predictions of the final *V* in mature ice. The observation that the depth of bubble closure controls the magnitude of the resulting *V* has important implications for the interpretation of air content as a proxy for paleo-ice sheet elevation.

First, the magnitude of density variability at the top of the LIZ will affect *V* because it will increase the amount of shallowly trapped bubbles.

Second, our parameterization does not consider interaction between adjacent firn layers, which will occur in real firn. *Stauffer et al*. [1985] observed that dense winter layers can form impermeable barriers that trap air in the open summer layers below, causing the latter to have higher *V*. By drilling and cutting firn samples, pore clusters can be opened that were effectively sealed in the undisturbed firn. The parameterizations are fitted to the closed porosity in disturbed samples. Layering leads to a shallower effective sealing depth compared to the depth where full closure is predicted in our parameterization. The deepest firn sampling depth may not be a reliable gage for the effective sealing depth, given that extensive lateral connectivity (from which air can be pumped) can remain below such sealing layers. The sealing effect implies that strongly layered firn retains more air than firn which is more homogenous.

Third, the magnitude of density variability might be a confounding variable that introduces noise into the relationship between the mature *V* and the mean site temperature [*Delmotte et al*., 1999; *Martinerie et al*., 1994]. A new parameterization that accounts for the magnitude of density variability and then relates *V* to mean site temperature could yield a higher correlation.

Finally, recent work on high-resolution density and trace element records shows that densification rates are correlated with chemical impurities in the ice leading to the hypothesis that high concentrations of chemical impurities induce softening of the firn and, therefore, control densification processes [*Freitag et al*., 2013; *Hörhold et al*., 2012]. We observe similar correlations of trace element and chemical impurities with density in our LIZ samples (section 3.1). Since chemical impurities vary by orders of magnitude on glacial-interglacial time scales, it is possible that impurities are impacting *V* through changes in the magnitude of density variability. This could complicate the interpretation of *V* as a surface elevation proxy. The impurity content of the ice may merely be colocated with another parameter that is controlling the densification processes such as microstructural properties retained at depth from surface characteristics [*Gregory et al*., 2014], and further work is needed to understand these relationships.

4.3. Recommendations for Further Studies

These initial results call for further investigation, and the following are recommended modifications to the experimental design. (1) Field-based CH_4 analysis using a discrete sampling technique would reduce the possibility of postcoring entrapment of modern air and could be compared with lab-based results of CH_4 and $\delta^{15}N$ conducted later to quantify the degree of postcoring contamination. Alternatively, packing samples in a vacuum container in the field for later analysis in the lab could accomplish the same goals. (2) Colocated measurements of chemical impurities would allow for a detailed investigation of the impact on *V*.

(3) Colocated measurements of physical properties of the ice and pore volume would allow for a comparison with V and verify the bubble compaction parameterization. (4) These measurements should be conducted at sites with a large range of temperature, accumulation, density variability, LIZ thickness, and trace element loading characteristics in order to validate the parameterization for climatically dissimilar conditions.

5. Conclusions

Measurements of methane and total air content (V) from within the lock-in zone (LIZ) in a WAIS Divide core reveal large anticorrelated variations indicating that layering is causing bubble trapping to occur in a staggered manner throughout the LIZ. Until now layering of the firn had not been incorporated in firn air transport models in a systematic way. Previous work on firn air modeling used parameterizations for bubble trapping based on centimeter-scale samples representing local ice properties (ρ, s) and applied these parameterizations to bulk ice properties ($<\rho>$, $<s>$). This approach is strictly speaking invalid because high-frequency layering within the firn causes bubble trapping to occur over a wider depth range than predicted by the bulk density profile alone. We use the original parameterization for local closed porosity (s_{cl}) convolved with a Gaussian distribution with a width defined by the magnitude of density variability to represent the effects of high-frequency layering. This new stochastic parameterization has a physical basis, is computationally inexpensive, and yields an improved fit to a variety of firn parameters including bulk closed pore volume ($<s_{cl}>$), V, and CH_4 in the closed porosity. At WAIS Divide, it also correctly predicts that there is finite open porosity at the depth of the deepest extraction of air from the open porosity, as opposed to the other parameterizations which predict that all of the pores are fully closed at that depth, and thus need an ad hoc modification in order to fit the observations. Our CH_4 data provide a constraint on the mean age of the air in the closed porosity at the base of the LIZ and show that the commonly used ad hoc modification to the porosity parameterization affects the depth at which bubbles close and yields a mean age that is too young. We also calculate the variability of the mean age from the high-resolution density and show that this causes peak-to-peak variations in the mean gas age of ~10 years. This variability is consistent with observations from other ice cores and indicates that quasi-annual variations of methane seen in high-resolution (centimeter-scale) measurements result from density layering in the firn and not from a high-frequency atmospheric signal.

Our stochastic parameterization also has implications for the interpretation of V records and estimates of past ice sheet thickness. The V is affected by the depth at which bubbles close and by the magnitude of density variability in the ice. Relating these observations to chemical impurities in the ice and detailed firn microstructure could help explain some of the observed variability in V records on a range of time scales and could assist in using V in other applications such as astronomical dating of ice cores [*Raynaud et al.*, 2007]. Finally, we return to the paradox mentioned in section 1 that the observed smoothing of methane records from ice cores is much less than would be expected from the depth interval over which bubbles close off. We suggest that the resolution to the paradox is that vertical diffusion of gas is nearly prevented by impermeable horizontal layers in the lock-in zone, before most of the bubbles are closed off. This restricts further age broadening of the gas due to gradual bubble closure within the lock-in zone, by preventing younger air from penetrating into the regions where most bubbles are closing off. Because modeling efforts generally follow the common practice of using empirical diffusivities [e.g., *Buizert et al.*, 2012], they already contain implicitly the narrowing effect of layering on the age distribution. Our model improvements in the present work have found a slight broadening relative to earlier models, but it should be made clear that the total net effect of layering on gas trapping and the width of the age distribution of gases are unquestionably to narrow the age distribution in resolution of the paradox.

Acknowledgments

This work was supported by NSF OPP grants 0538578, 0520523, 0538538, 0944343 (to J.P.S.), 0944078 (to M.R.A.), 1142166 (to J.R.M.), and 1043528 (to R.B.A.), the NASA/Oregon Space Grant Consortium grant NNG05GJ85H (to L.E.M.), the NOAA Climate and Global Change Fellowship Program, administered by the University Corporation for Atmospheric Research (to C.B.), and the Polar Academic Program (PAP, PD12010) of Korea Polar Research Institute (KOPRI). We thank Brendan Williams, James Lee, and Jon Edwards for assisting in sample preparation and analysis at OSU; N. Chellman and L. Layman for help in the continuous analyses at DRI; Max Stevens for checking the porosity parameterization equations; Jakob Schwander and David Etheridge for useful discussions and sharing porosity data; Steve Montzka for sharing WAIS halocarbon firn air data; the University of Wisconsin-Madison Automatic Weather Station Program for the surface pressure observations from Kominko-Slade AWS (NSF grants ANT-0944018 and ANT-1245663); two anonymous reviewers for constructive comments which improved the clarity of the manuscript; the WAIS Divide Science Coordination Office at DRI, Reno, Nevada, for the collection and distribution of the WAIS Divide ice core (Kendrick Taylor, NSF grants 0230396, 0440817, 0944348, and 0944266—University of New Hampshire); NSF OPP which funds the Ice Drilling Program Office and Ice Drilling Design and Operations group for coring activities; NSF which funds the National Ice Core Laboratory which curated and processed the core; Raytheon Polar Services which provided logistics support in Antarctica; and the 109th New York Air National Guard for airlift in Antarctica. Data and description can be downloaded from the NOAA National Climate Data Center http://www.ncdc.noaa.gov/data-access/paleoclimatology-data.

References

Adolph, A. C., and M. R. Albert (2013), The physical basis for gas transport through polar firn: A case study at Summit, Greenland, *Cryosphere Discuss.*, *7*(3), 2455–2487.

Ahn, J., E. J. Brook, and C. Buizert (2013), Response of atmospheric CO_2 to the abrupt cooling event 8200 years ago, *Geophys. Res. Lett.*, *41*, 604–609, doi:10.1002/2013GL058177.

Aydin, M., et al. (2010), Post-coring entrapment of modern air in some shallow ice cores collected near the firn-ice transition: Evidence from CFC-12 measurements in Antarctic firn air and ice cores, *Atmos. Chem. Phys.*, *10*(11), 5135–5144.

Banta, J. R., J. R. McConnell, M. M. Frey, R. C. Bales, and K. Taylor (2008), Spatial and temporal variability in snow accumulation at the West Antarctic Ice Sheet Divide over recent centuries, *J. Geophys. Res.*, *113*, D23102, doi:10.1029/2008JD010235.

Battle, M., et al. (1996), Atmospheric gas concentrations over the past century measured in air from firn at the South Pole, *Nature*, *383*(6597), 231–235.
Battle, M., J. P. Severinghaus, E. D. Sofen, D. Plotkin, A. J. Orsi, M. Aydin, S. A. Montzka, T. Sowers, and P. P. Tans (2011), Controls on the movement and composition of firn air at the West Antarctic Ice Sheet Divide, *Atmos. Chem. Phys.*, *11*(21), 11,007–11,021.
Breton, D. J., G. S. Hamilton, and C. T. Hess (2009), Design, optimization and calibration of an automated density gauge for firn and ice cores, *J. Glaciol.*, *55*, 1092–1100.
Buizert, C. (2011), The influence of firn air transport processes and radiocarbon production on gas records from polar firn and ice, Univ. of Copenhagen.
Buizert, C. (2013), Studies of firn air, in *The Encyclopedia of Quaternary Science*, edited by S. A. Elias, pp. 361–372, Elsevier, Amsterdam, Netherlands.
Buizert, C., et al. (2012), Gas transport in firn: Multiple-tracer characterisation and model intercomparison for NEEM, Northern Greenland, *Atmos. Chem. Phys.*, *12*(9), 4259–4277.
Buizert, C., T. Sowers, and T. Blunier (2013), Assessment of diffusive isotopic fractionation in polar firn, and application to ice core trace gas records, *Earth Planet. Sci. Lett.*, *361*, 110–119.
Delmotte, M., D. Raynaud, V. Morgan, and J. Jouzel (1999), Climatic and glaciological information inferred from air-content measurements of a Law Dome (East Antarctica) ice core, *J. Glaciol.*, *45*(150), 255–263.
Etheridge, D. M., G. I. Pearman, and P. J. Fraser (1992), Changes in tropospheric methane between 1841 and 1978 from a high accumulation rate Antarctic ice core, *Tellus B*, *44*(4), 282–294.
Etheridge, D. M., L. P. Steele, R. J. Francey, and R. L. Langenfelds (1998), Atmospheric methane between 1000 AD and present: Evidence of anthropogenic emissions and climatic variability, *J. Geophys. Res.*, *103*(D13), 15,979–15,993, doi:10.1029/98JD00923.
Freitag, J., F. Wilhelms, and S. Kipfstuhl (2004), Microstructure-dependent densification of polar firn derived from X-ray microtomography, *J. Glaciol.*, *50*(169), 243–250.
Freitag, J., J. Kipfstuhl, T. Laepple, and F. Wilhelms (2013), Impurity-controlled densification: A new model for stratified polar firn, *J. Glaciol.*, *59*(218), 1163–1169.
Gerland, S., H. Oerter, J. Kippstuhl, F. Wilhelms, H. Miller, and W. D. Miners (1999), Density log of a 181 m long ice core from Berkner Island, Antarctica, in *Annals of Glaciology*, vol. 29, edited by T. H. Jacka, pp. 215–219, Int. Glaciol. Soc., Cambridge, U. K.
Goujon, C., J. M. Barnola, and C. Ritz (2003), Modeling the densification of polar firn including heat diffusion: Application to close-off characteristics and gas isotopic fractionation for Antarctica and Greenland sites, *J. Geophys. Res.*, *108*(D24), doi:10.1029/2002JD003319.
Gregory, S. A., M. R. Albert, and I. Baker (2014), Impact of physical properties and accumulation rate on pore close-off in layered firn, *Cryosphere*, *8*(1), 91–105.
Hörhold, M. W., S. Kipfstuhl, F. Wilhelms, J. Freitag, and A. Frenzel (2011), The densification of layered polar firn, *J. Geophys. Res.*, *116*, F01001, doi:10.1029/2009JF001630.
Hörhold, M. W., T. Laepple, J. Freitag, M. Bigler, H. Fischer, and S. Kipfstuhl (2012), On the impact of impurities on the densification of polar firn, *Earth Planet. Sci. Lett.*, *325–326*, 93–99.
Kalambet, Y., Y. Kozmin, K. Mikhailova, I. Nagaev, and P. Tikhonov (2011), Reconstruction of chromatographic peaks using the exponentially modified Gaussian function, *J. Chemom.*, *25*(7), 352–356.
Kawamura, K., J. P. Severinghaus, S. Ishidoya, S. Sugawara, G. Hashida, H. Motoyama, Y. Fujii, S. Aoki, and T. Nakazawa (2006), Convective mixing of air in firn at four polar sites, *Earth Planet. Sci. Lett.*, *244*(3–4), 672–682.
Kreutz, K., B. Koffman, D. Breton, and G. S. Hamilton (2011), Microparticle, conductivity, and density measurements from the WAIS Divide Deep Ice Core, Antarctica.
Lazzara, M. A., G. A. Weidner, L. M. Keller, J. E. Thom, and J. J. Cassano (2012), Antarctic Automatic Weather Station Program: 30 years of polar observation, *Bull. Am. Meteorol. Soc.*, *93*(10), 1519–1537.
Lipenkov, V., F. Candaudap, J. Ravoire, E. Dulac, and D. Raynaud (1995), A new device for the measurement of air content in polar ice, *J. Glaciol.*, *41*(138), 423–429.
Loulergue, L., A. Schilt, R. Spahni, V. Masson-Delmotte, T. Blunier, B. Lemieux, J. M. Barnola, D. Raynaud, T. F. Stocker, and J. Chappellaz (2008), Orbital and millennial-scale features of atmospheric CH_4 over the past 800,000 years, *Nature*, *453*(7193), 383–386.
Luthi, D., et al. (2008), High-resolution carbon dioxide concentration record 650,000-800,000 years before present, *Nature*, *453*(7193), 379–382.
Martinerie, P., D. Raynaud, D. M. Etheridge, J. M. Barnola, and D. Mazaudier (1992), Physical and climatic parameters which influence the air content in polar ice, *Earth Planet. Sci. Lett.*, *112*(1–4), 1–13.
Martinerie, P., V. Y. Lipenkov, D. Raynaud, J. Chappellaz, N. I. Barkov, and C. Lorius (1994), Air content paleo record in the Vostok ice core (Antarctica): A mixed record of climatic and glaciological parameters, *J. Geophys. Res.*, *99*(D5), 10,565–10,576, doi:10.1029/93JD03223.
McConnell, J. R. (2002), Continuous ice-core chemical analyses using inductively coupled plasma mass spectrometry, *Environ. Sci. Technol.*, *36*(1), 7–11.
McConnell, J. R., R. Edwards, G. L. Kok, M. G. Flanner, C. S. Zender, E. S. Saltzman, J. R. Banta, D. R. Pasteris, M. M. Carter, and J. D. W. Kahl (2007), 20th-century industrial black carbon emissions altered arctic climate forcing, *Science*, *317*(5843), 1381–1384.
Mitchell, L. E., E. J. Brook, T. Sowers, J. R. McConnell, and K. Taylor (2011), Multidecadal variability of atmospheric methane, 1000–1800 CE, *J. Geophys. Res.*, *116*, G02007, doi:10.1029/2010JG001441.
Mitchell, L., E. Brook, J. E. Lee, C. Buizert, and T. Sowers (2013), Constraints on the Late Holocene anthropogenic contribution to the atmospheric methane budget, *Science*, *342*(6161), 964–966.
Orsi, A. J., B. D. Cornuelle, and J. P. Severinghaus (2012), Little Ice Age cold interval in West Antarctica: Evidence from borehole temperature at the West Antarctic Ice Sheet (WAIS) Divide, *Geophys. Res. Lett.*, *39*, L09710, doi:10.1029/2012GL051260.
Petrenko, V. V., J. P. Severinghaus, E. J. Brook, N. Reeh, and H. Schaefer (2006), Gas records from the West Greenland ice margin covering the Last Glacial Termination: A horizontal ice core, *Quat. Sci. Rev.*, *25*(9–10), 865–875.
Raynaud, D., and I. M. Whillans (1982), Air content of the byrd core and past changes in the West Antarctic Ice Sheet, *Ann. Glaciol.*, *3*, 269–273.
Raynaud, D., J. Chappellaz, C. Ritz, and P. Martinerie (1997), Air content along the Greenland Ice Core Project core: A record of surface climatic parameters and elevation in central Greenland, *J. Geophys. Res.*, *102*(C12), 26,607–26,613, doi:10.1029/97JC01908.
Raynaud, D., V. Lipenkov, B. Lemieux-Dudon, P. Duval, M. F. Loutre, and N. Lhomme (2007), The local insolation signature of air content in Antarctic ice. A new step toward an absolute dating of ice records, *Earth Planet. Sci. Lett.*, *261*(3–4), 337–349.
Rhodes, R. H., X. Faïn, C. Stowasser, T. Blunier, J. Chappellaz, J. R. McConnell, D. Romanini, L. E. Mitchell, and E. J. Brook (2013), Continuous methane measurements from a late Holocene Greenland ice core: Atmospheric and in-situ signals, *Earth Planet. Sci. Lett.*, *368*, 9–19.
Schwander, J. (1989), The transformation of snow to ice and the occlusion of gases, in *The Environmental Record in Glaciers and Ice Sheets*, edited by H. Oeschger and C. C. Langway, pp. 53–67, John Wiley, Chichester [England]; New York.
Schwander, J., and B. Stauffer (1984), Age difference between polar ice and the air trapped in its bubbles, *Nature*, *311*(5981), 45–47.

Schwander, J., J. M. Barnola, C. Andrie, M. Leuenberger, A. Ludin, D. Raynaud, and B. Stauffer (1993), The age of the air in the firn and the ice at Summit, Greenland, *J. Geophys. Res.*, *98*(D2), 2831–2838, doi:10.1029/92JD02383.

Severinghaus, J. P., and M. O. Battle (2006), Fractionation of gases in polar ice during bubble close-off: New constraints from firn air Ne, Kr and Xe observations, *Earth Planet. Sci. Lett.*, *244*(1–2), 474–500.

Severinghaus, J. P., R. Beaudette, M. A. Headly, K. Taylor, and E. J. Brook (2009), Oxygen-18 of O_2 records the impact of abrupt climate change on the terrestrial biosphere, *Science*, *324*(5933), 1431–1434.

Severinghaus, J. P., et al. (2010), Deep air convection in the firn at a zero-accumulation site, central Antarctica, *Earth Planet. Sci. Lett.*, *293*(3–4), 359–367.

Sowers, T., M. Bender, and D. Raynaud (1989), Elemental and isotopic composition of occluded O_2 and N_2 in polar ice, *J. Geophys. Res.*, *94*(D4), 5137–5150, doi:10.1029/JD094iD04p05137.

Sowers, T., M. Bender, D. Raynaud, and Y. S. Korotkevich (1992), $\delta^{15}N$ of N_2 in air trapped in polar ice: A tracer of gas transport in the fim and a possible constraint on ice age-gas age differences, *J. Geophys. Res.*, *97*(D14), 15,683–15,697, doi:10.1029/92JD01297.

Spahni, R., J. Schwander, J. Fluckiger, B. Stauffer, J. Chappellaz, and D. Raynaud (2003), The attenuation of fast atmospheric CH_4 variations recorded in polar ice cores, *Geophys. Res. Lett.*, *30*(11), 1571, doi:10.1029/2003GL017093.

Stauffer, B., J. Schwander, and H. Oeschger (1985), Enclosure of air during metamorphosis of dry firn to ice, *Ann. Glaciol.*, *6*, 108–112.

Stowasser, C., et al. (2012), Continuous measurements of methane mixing ratios from ice cores, *Atmos. Meas. Tech.*, *5*(5), 999–1013.

Trudinger, C. M., I. G. Enting, D. M. Etheridge, R. J. Francey, V. A. Levchenko, L. P. Steele, D. Raynaud, and L. Arnaud (1997), Modeling air movement and bubble trapping in firn, *J. Geophys. Res.*, *102*(D6), 6747–6763, doi:10.1029/96JD03382.

Trudinger, C. M., D. M. Etheridge, P. J. Rayner, I. G. Enting, G. A. Sturrock, and R. L. Langenfelds (2002), Reconstructing atmospheric histories from measurements of air composition in firn, *J. Geophys. Res.*, *107*(D24), 4780, doi:10.1029/2002JD002545.

Witrant, E., et al. (2012), A new multi-gas constrained model of trace gas non-homogeneous transport in firn: Evaluation and behaviour at eleven polar sites, *Atmos. Chem. Phys.*, *12*(23), 11,465–11,483.